ChemComm

Chemical Communications

rsc.li/chemcomm

ROYAL SOCIETY
OF CHEMISTRY

COMMUNICATION
Takeharu Haino *et al*.
Supramolecular chiral sensing by supramolecular helical polymers

COMMUNICATION

Check for updates

Supramolecular chiral sensing by supramolecular helical polymers†

Takehiro Hirao,‡[a] Sei Kishino‡[a] and Takeharu Haino [ID] *[ab]

A tetrakis(porphyrin) with branched side chains self-assembled to form supramolecular helical polymers both in solution and in the solid state. The helicity of the supramolecular polymers was determined by the chirality of solvent molecules, which permitted the polymer chains to be used in chiral sensing.

Molecular sensors consist of a broad and diverse subset of chromogenic and fluorogenic molecules.[1–8] When they interact with analytes, their characteristic absorption and/or emission bands are changed. These spectral changes can be readout signals that are readable by using spectroscopic means as well as the naked eye. Among many target analytes, much research attention has been directed toward detecting chiral molecules, such as hydrocarbons, amines, amino alcohols, and amino acids.[9,10] Electronic circular dichroism (ECD), X-ray crystallography, and nuclear magnetic resonance (NMR) are commonly used to determine the absolute chiralities of molecules. However, the above methods are often hampered when detecting absolute chiralities of chiral molecules with no appreciable absorption in the UV/vis region. Recent efforts have been devoted to developing new technologies to determine the absolute structures of such chiral molecules. Fujita *et al.* reported that metal–organic frameworks encapsulated chiral molecules and the chiralities were directly determined by X-ray crystallographic analysis, the so-called "crystalline sponge method."[11–14] When chiral molecules possess functional groups available for anchoring chiral auxiliary or chromogenic units, NMR and ECD methods become potential strategies.[15–19] Supramolecular chemistry offers a unique and easy way to unveil the

hidden chiral information in the chiral molecules by using the ECD probes.[20–27] Although chiralities are easily detected based on the supramolecular method using ECD probes, the method commonly requires interactive heteroatoms within the analyte molecules. Thus, achieving facile detection of chiralities remains an essential scientific challenge with high sensitivity, particularly for pure hydrocarbons.

Supramolecular polymers are formed through the molecular association of supramolecular monomers.[28–33] Appropriately designed supramolecular monomers self-assemble to form helical supramolecular polymers.[34–39] Due to the manner of their connection, the helix sense within the helical polymer chains is in equilibrium between plus- and minus-helices. The equilibrium is known to be imbalanced by the addition of nonracemic molecules to the solution.[40–43] Thus, due to their dynamic helicity, supramolecular polymers show promise as chiral sensors in which the chiral information of the analytes is outputted as the helix sense of the polymer chains.

Covalently linked tetrakis(porphyrin) **1**, in which two bis(porphyrin) moieties are connected, forms helical supramolecular
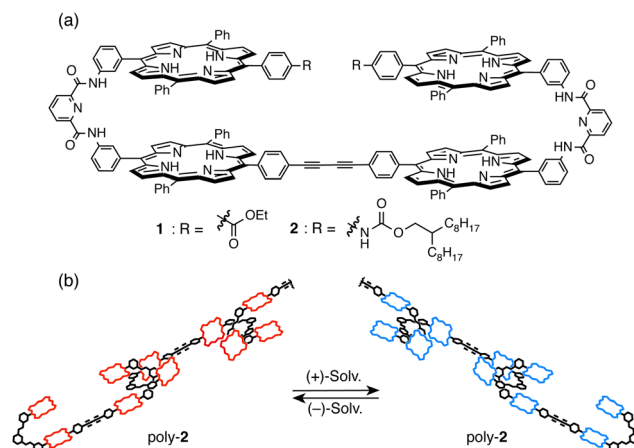
[a] *Department of Chemistry, Graduate School of Advanced Science and Engineering, Hiroshima University, 1-3-1, Kagamiyama, Higashi-Hiroshima 739-8526, Japan. E-mail: haino@hiroshima-u.ac.jp*

[b] *International Institute for Sustainability with Knotted Chiral Meta Matter (SKCM², Hiroshima University, 1-3-1 Kagamiyama, Higashi-Hiroshima, 739-8526, Japan*

† Electronic supplementary information (ESI) available. See DOI: https://doi.org/10.1039/d2cc06502a

‡ These authors contributed equally.

Fig. 1 (a) Molecular structures of tetrakis(porphyrin) **1** and **2**. (b) Schematic illustration of the formation of supramolecular polymer poly-**2**.

polymers by utilizing bis(porphyrin)–bis(porphyrin) self-complementary pairing interactions in an iterative fashion (Fig. 1).[44–46] We envisioned that the helix sense of tetrakis(porphyrin) could be biased by the external chirality; this can be a chiral detection system in which the biased helix sense can be read by an ECD spectrometer due to the intense absorption of the porphyrin moieties. Here, we report the transference of the chirality within pure hydrocarbons to the helix comprised of **2**.

We newly designed tetrakis(porphyrin) **2** with branched alkyl chains in the periphery to improve its solubility toward hydrocarbons (Fig. S1–S4, ESI†). Prior to studying the chiral detection capability, the self-assembly behavior of **2** was studied. **2** exhibited a characteristic absorption band at 420 nm that was assignable to the Soret band of porphyrins at 90 °C in toluene (Fig. 2a). Upon cooling the solution, a new band at approximately 435 nm was observed to grow while decreasing the absorption at 420 nm, which suggests the molecular association of **2** in the solution.[44] The size of the assembled **2** was determined by evaluating diffusion coefficient (D) values at various concentrations (Fig. 2b and Fig. S5, ESI†). Diffusion-ordered ^{1}H NMR spectroscopy (DOSY) provided D values of **2** at concentrations up to 30 mmol L^{-1} in chloroform-d. The D value decreased upon concentrating the solution. An inversely proportional relation between D and the molecular size is described in the Stokes–Einstein equation; thus, the decrease in D values indicates that supramolecular polymers formed in solution.

Atomic force microscopy (AFM) and high-resolution mass spectrometry (HRMS) support that the supramolecular polymer poly-**2** formed. Polymeric fibrous morphologies were visualized

in the AFM images of the cast films of **2**, which were prepared from its 1,2-dichloroethane solution on highly oriented pyrolytic graphite (HOPG) (Fig. 2c and d). The HRMS spectrum displayed signals corresponding to the dimer and trimer of **2** (Fig. S6, ESI†). These results led to the conclusion that **2** forms supramolecular polymer poly-**2** both in solution and in the solid state, analogous to that previously reported for **1**.

To discuss the sensing capability of the supramolecular polymer poly-**2**, enantiopure limonene and **2** were mixed in quartz cuvettes and subjected to ECD measurements. A mirror image relationship was illustrated between the ECD spectra obtained from the (+)-limonene solution of **2** and the (−)-limonene solution of **2** (Fig. 3a). Limonene exhibits a negligible absorption intensity in the wavelength region of 350–800 nm; thus, this observation clearly suggests that chiral information of limonene is transferred to poly-**2**; as a result, a chirally twisted conformation is induced within the polymer chains of poly-**2**, which is readable by an ECD spectrometer. To corroborate that the chiral information of limonene was transferred to poly-**2**, the self-association constant of **2** in (+)-limonene was estimated by monitoring changes in the UV/vis absorption band. Although the extremely high self-association affinity of **2** in limonene prevented the self-association constant from being determined at 25 °C, the curve fitting analysis[47–49] indicated the self-association constant (K_a) was $(1.2 ± 0.2) × 10^7$ L mol^{-1} at 90 °C (Fig. 3b and Fig. S7, ESI†). Based on the K_a value, approximately 18 molecules are connected at the concentration of $2.5 × 10^{-5}$ mol L^{-1} at 90 °C; thus, more than 18-mer[50] should be formed in the solution at 25 °C; based on these results, the helical conformation within the supramolecular polymer chain is biased by the chirality of limonene to emerge the ECD band in the detectable wavelength region.

Discernible ECD bands derived from the porphyrin moieties of **2** were observed when mixed with (−)-α-pinene and (−)-β-pinene (Fig. 4a). The ECD intensity was decreased upon heating the solution (Fig. S9, ESI†); thus, the chiral information of pinenes was displayed as one-handed helicity of helical polymer poly-**2**, which can be read by an ECD spectrometer. The ECD intensity was seen to diminish upon decreasing the
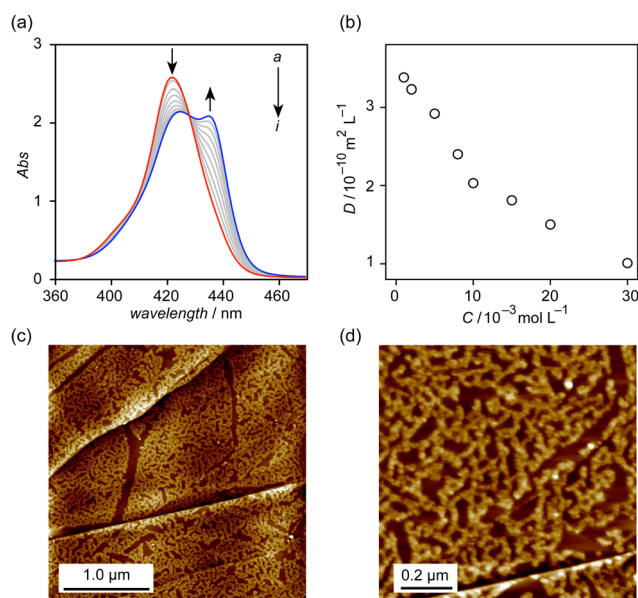

Fig. 2 (a) Valuable temperature UV/vis absorption spectra of **2** in toluene at a concentration of $2.2 × 10^{-6}$ mol L^{-1}. The temperatures are (a–i) 90, 80, 70, 60, 50, 40, 30, 20, and 10 °C. The red and blue lines denote the spectra observed at 90 °C and 10 °C, respectively. (b) Plot of diffusion coefficient (D) values of **2** in chloroform-d. (c and d) AFM images of the cast films of **2** on HOPG prepared from its 1,2-dichloroethane solution.
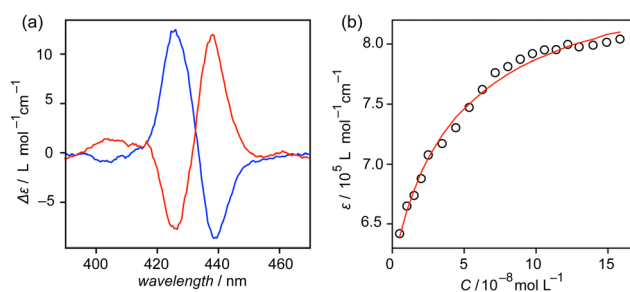

Fig. 3 (a) ECD spectra of **2** ($2.5 × 10^{-5}$ mol L^{-1}) in (red) (+)-limonene and (blue) (−)-limonene at room temperature. (b) Binding isotherm analysis corresponding to the formation of intermolecular bis(porphyrin)–bis(porphyrin) self-complementary pairs of **2** in an iterative fashion in (+)-limonene at 90 °C. The plotted extinction coefficient (ε) values are $\lambda = 435$ nm. The full spectra are shown in Fig. S7 (ESI†).
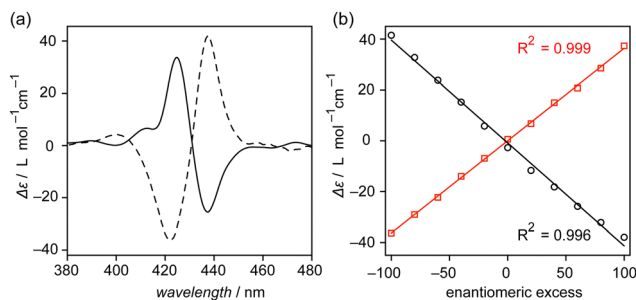
Fig. 4 (a) ECD spectra of **2** (2.5×10^{-5} mol L^{-1}) in (dashed line) $(-)$-α-pinene and (solid line) $(-)$-β-pinene at room temperature. (b) Linear correlation between ee and $\Delta\varepsilon$ value of **2** (2.5×10^{-5} mol L^{-1}) at (red) 422 nm and (black) 437 nm observed in α-pinene. Enantiomeric excess = $\{([(+)\text{-}\alpha\text{-pinene}] - [(-)\text{-}\alpha\text{-pinene}])/([(+)\text{-}\alpha\text{-pinene}] + [(-)\text{-}\alpha\text{-pinene}])\} \times 100$. The full spectra are shown in Fig. S10 (ESI†).

enantiomeric excess (ee) of α-pinene (Fig. S10, ESI†). A perfect linearity with the calculated R^2 values over 0.995 was clearly illustrated in the plot of ECD intensities of **2** at 422 nm and 437 nm against ee of α-pinene (Fig. 4b). The linear correlation can be used to precisely detect the ee of α-pinene. $(+)$- and $(-)$-α-pinenes were mixed in prechosen enantiomeric ratios and subjected to ECD measurements. The ee values of the specimens were estimated from their $\Delta\varepsilon$ values at 422 nm based on the linear formula (Fig. S11, ESI†) obtained from the plot shown in Fig. 4b. All estimated values were in good agreement with the actual values calculated from their compositions, in which the absolute error values were within $\pm4\%$ (Table 1). The absolute error values are sufficiently small[18,27] that poly-**2** can be used as a chiral sensor.

To determine the limit of detection (LOD) of the poly-**2** based sensing system, ECD spectra of **2** were monitored in $(-)$-α-pinene/toluene and $(-)$-α-pinene/chloroform mixtures. As can be seen in the ECD spectra (Fig. 5), monotonical decreases in the ECD intensity were observed upon diluting $(-)$-α-pinene by toluene and chloroform. Judging from the ECD intensities, at least 60% of α-pinene content in the organic media is required to sense the chirality of α-pinene.

In summary, we demonstrated the synthesis of tetrakis(porphyrin) **2**, which contains branched alkyl chains in the periphery, and its self-assembling behaviors. **2** self-assembled to form linear supramolecular polymers both in solution and in the solid state,

Fig. 5 (a) ECD spectra of **2** (2.5×10^{-5} mol L^{-1}) in (a) $(-)$-α-pinene/toluene mixture and (b) $(-)$-α-pinene/chloroform mixture. The mixing ratios of $(-)$-α-pinene: solvents are (a–e) $10:0$, $8:2$, $6:4$, $4:6$, $2:8$ (v/v).

which is consistent with a previously reported tetrakis(porphyrin). The chiral information of limonene, α-pinene, and β-pinene was transferred to assembled **2** as its helical chirality, which can be read by an ECD spectrometer. Notably, linear correlation with the correlation coefficient $R^2 =$ over 0.995 was illustrated in the plot of the ECD intensities against the ee of α-pinene, providing promise in determining ee of the analyte. With the present approach, the ee values of α-pinene were detected within $\pm4\%$ accuracy of their actual values. Supramolecular chiral sensors for pure hydrocarbons based on ECD probes have been limited so far; thus, the present work sets the stage for creating new molecular sensors that can detect the chirality of pure hydrocarbon molecules.

Conflicts of interest

There are no conflicts to declare.

Notes and references

1 B. T. Nguyen and E. V. Anslyn, *Coord. Chem. Rev.*, 2006, **250**, 3118–3127.
2 A. T. Wright and E. V. Anslyn, *Chem. Soc. Rev.*, 2006, **35**, 14–28.
3 M. H. Lee, J. S. Kim and J. L. Sessler, *Chem. Soc. Rev.*, 2015, **44**, 4185–4191.
4 J. Wu, B. Kwon, W. Liu, E. V. Anslyn, P. Wang and J. S. Kim, *Chem. Rev.*, 2015, **115**, 7893–7943.
5 D. Wu, A. C. Sedgwick, T. Gunnlaugsson, E. U. Akkaya, J. Yoon and T. D. James, *Chem. Soc. Rev.*, 2017, **46**, 7105–7123.
6 T. L. Mako, J. M. Racicot and M. Levine, *Chem. Rev.*, 2019, **119**, 322–477.
7 C. Guo, A. C. Sedgwick, T. Hirao and J. L. Sessler, *Coord. Chem. Rev.*, 2021, **427**, 213560.
8 A. C. Sedgwick, J. T. Brewster, T. Wu, X. Feng, S. D. Bull, X. Qian, J. L. Sessler, T. D. James, E. V. Anslyn and X. Sun, *Chem. Soc. Rev.*, 2021, **50**, 9–38.

Table 1 Summary of the chiral sensing results for α-pinene and the absolute error values

Entry	ee[a] (%)	Estimated ee[b] (%)	Error (%)
1	72.0	68.2	−3.8
2	44.0	45.2	1.2
3	18.3	15.7	−2.6
4	−12.0	−9.18	2.8
5	−44.3	−41.4	2.9
6	−70.8	−68.7	2.1

[a] ee values calculated from the composition of $(+)$- and $(-)$-α-pinenes.
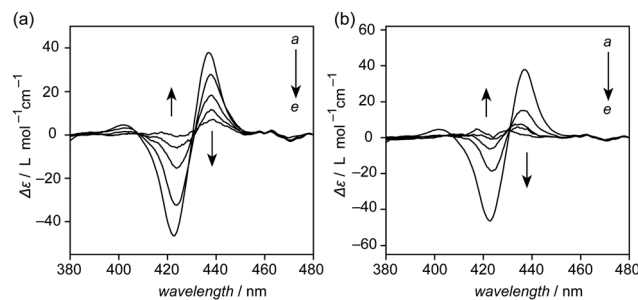[b] ee values estimated from the observed ECD intensity by using the linear equation (Fig. S11, ESI).

9 K. Mislow and P. Bickart, *Isr. J. Chem.*, 1977, **15**, 1–5.

10 K. Mislow, *Collect. Czech. Chem. Commun.*, 2003, **68**, 849–864.

11 Y. Inokuma, S. Yoshioka, J. Ariyoshi, T. Arai, Y. Hitora, K. Takada, S. Matsunaga, K. Rissanen and M. Fujita, *Nature*, 2013, **495**, 461–466.

12 Y. Inokuma, S. Yoshioka, J. Ariyoshi, T. Arai and M. Fujita, *Nat. Protoc.*, 2014, **9**, 246–252.

13 M. Hoshino, A. Khutia, H. Xing, Y. Inokuma and M. Fujita, *IUCrJ*, 2016, **3**, 139–151.

14 N. Zigon, V. Duplan, N. Wada and M. Fujita, *Angew. Chem., Int. Ed.*, 2021, **60**, 25204–25222.

15 D. Parker, *Chem. Rev.*, 1991, **91**, 1441–1457.

16 J. M. Seco, E. Quiñoá and R. Riguera, *Chem. Rev.*, 2004, **104**, 17–118.

17 T. R. Hoye, C. S. Jeffrey and F. Shao, *Nat. Protoc.*, 2007, **2**, 2451–2458.

18 C. Wolf and K. W. Bentley, *Chem. Soc. Rev.*, 2013, **42**, 5408–5424.

19 H. H. Jo, C.-Y. Lin and E. V. Anslyn, *Acc. Chem. Res.*, 2014, **47**, 2212–2221.

20 Y. Kikuchi, K. Kobayashi and Y. Aoyama, *J. Am. Chem. Soc.*, 1992, **114**, 1351–1358.

21 K. Kobayashi, Y. Asakawa, Y. Kikuchi, H. Toi and Y. Aoyama, *J. Am. Chem. Soc.*, 1993, **115**, 2648–2654.

22 L. Pu, *Chem. Rev.*, 2004, **104**, 1687–1716.

23 G. A. Hembury, V. V. Borovkov and Y. Inoue, *Chem. Rev.*, 2008, **108**, 1–73.

24 Z. Chen, Q. Wang, X. Wu, Z. Li and Y.-B. Jiang, *Chem. Soc. Rev.*, 2015, **44**, 4249–4263.

25 Y. Nagata, R. Takeda and M. Suginome, *ACS Cent. Sci.*, 2019, **5**, 1235–1240.

26 E. Yashima and K. Maeda, *Bull. Chem. Soc. Jpn.*, 2021, **94**, 2637–2661.

27 M. Quan, X.-Y. Pang and W. Jiang, *Angew. Chem., Int. Ed.*, 2022, **61**, e202201258.

28 D. S. Kim and J. L. Sessler, *Chem. Soc. Rev.*, 2015, **44**, 532–546.

29 Y. Han, Y. Tian, Z. Li and F. Wang, *Chem. Soc. Rev.*, 2018, **47**, 5165–5176.

30 H. Li, Y. Yang, F. Xu, T. Liang, H. Wen and W. Tian, *Chem. Commun.*, 2019, **55**, 271–285.

31 T. Haino, *Polym. J.*, 2019, **51**, 303–318.

32 T. Hirao and T. Haino, *Chem. – Asian J.*, 2022, **17**, e202200344.

33 T. Hirao, *Polym. J.*, 2023, **55**, 95–104.

34 T. Ikeda, K. Hirano and T. Haino, *Mater. Chem. Front.*, 2018, **2**, 468–474.

35 T. Haino and T. Hirao, *Chem. Lett.*, 2020, **49**, 574–584.

36 P. K. Hashim, J. Bergueiro, E. W. Meijer and T. Aida, *Prog. Polym. Sci.*, 2020, **105**, 101250.

37 M. Wehner and F. Würthner, *Nat. Rev. Chem.*, 2020, **4**, 38–53.

38 T. Hirao, N. Fujii, Y. Iwabe and T. Haino, *Chem. Commun.*, 2021, **57**, 11831–11834.

39 T. Hirao, Y. Iwabe, N. Fujii and T. Haino, *J. Am. Chem. Soc.*, 2021, **143**, 4339–4345.

40 V. Stepanenko, X.-Q. Li, J. Gershberg and F. Würthner, *Chem. – Eur. J.*, 2013, **19**, 4176–4183.

41 M. L. Ślęczkowski, M. F. J. Mabesoone, P. Ślęczkowski, A. R. A. Palmans and E. W. Meijer, *Nat. Chem.*, 2021, **13**, 200–207.

42 S. Datta, S. Takahashi and S. Yagai, *Acc. Mater. Res.*, 2022, **3**, 259–271.

43 S. Yagai, *Nat. Nanotechnol.*, 2022, **17**, 1241–1242.

44 T. Fujii, A. Watanabe and U. Takayanagi, *Proc. Natl. Acad. Sci. U. S. A.*, 2009, **106**, 10477.

45 K. Nadamoto, K. Maruyama, N. Fujii, T. Ikeda, S.-I. Kihara and T. Haino, *Angew. Chem., Int. Ed.*, 2018, **57**, 7028–7033.

46 N. Hisano, T. Hirao, K. Tanabe and T. Haino, *J. Porphyrins Phthalocyanines*, 2022, **26**, 683–689.

47 R. B. Martin, *Chem. Rev.*, 1996, **96**, 3043–3064.

48 P. Jonkheijm, P. van der Schoot, A. P. H. J. Schenning and E. W. Meijer, *Science*, 2006, **313**, 80–83.

49 M. M. J. Smulders, M. M. L. Nieuwenhuizen, T. F. A. de Greef, P. van der Schoot, A. P. H. J. Schenning and E. W. Meijer, *Chem. – Eur. J.*, 2010, **16**, 362–367.

50 The AFM image prepared from (+)-limonene solution of 2 provided ridge and valley morphologies derived from bundled, thick polymer chains (Fig. S8, ESI†), supporting the formation of supramolecular polymers.